HHS Public Access

Author manuscript

Int J Non Linear Mech. Author manuscript; available in PMC 2016 November 01.

Published in final edited form as:

Int J Non Linear Mech. 2015 November ; 76: 135–143. doi:10.1016/j.ijnonlinmec.2015.06.001.

Free energy of the edge of an open lipid bilayer based on the interactions of its constituent molecules

Meisam Asgari[*] and **Aisa Biria**

Department of Mechanical Engineering, McGill University, Montréal, QC H3A 0C3, Canada

Abstract

Lipid-bilayers are the fundamental constituents of the walls of most living cells and lipid vesicles, giving them shape and compartment. The formation and growing of pores in a lipid bilayer have attracted considerable attention from an energetic point of view in recent years. Such pores permit targeted delivery of drugs and genes to the cell, and regulate the concentration of various molecules within the cell. The formation of such pores is caused by various reasons such as changes in cell environment, mechanical stress or thermal fluctuations. Understanding the energy and elastic behaviour of a lipid-bilayer edge is crucial for controlling the formation and growth of such pores. In the present work, the interactions in the molecular level are used to obtain the free energy of the edge of an open lipid bilayer. The resulted free-energy density includes terms associated with flexural and torsional energies of the edge, in addition to a line-tension contribution. The line tension, elastic moduli, and spontaneous normal and geodesic curvatures of the edge are obtained as functions of molecular distribution, molecular dimensions, cutoff distance, and the interaction strength. These parameters are further analyzed by implementing a soft-core interaction potential in the microphysical model. The dependence of the elastic free-energy of the edge to the size of the pore is reinvestigated through an illustrative example, and the results are found to be in agreement with the previous observations.

Keywords

Free energy; elasticity; open lipid bilayer; differential geometry; boundary curve of a surface; molecular interactions

1. Introduction

A phospholipid molecule consists of a hydrophilic head and two hydrophobic fatty-acid tails [1]. When suspended in an aqueous solution at sufficient concentrations, phospholipid molecules self-assemble into structures such as lipid bilayers, in order to shield the tail groups from the solvent [2, 3]. Lipid bilayers are the main constituents of cell membrane in most living organisms, as well as model membranes such as liposomes [4]. They provide the

[*] Corresponding author meisam.asgari@mail.mcgill.ca (Meisam Asgari).

cell and its substructures with compartment and shape, and further, function as barriers for water-soluble molecules such as water, ions, and proteins [5, 6]. Lipid bilayers are composed of two adjacent leaflets of phospholipid molecules oriented transversely and set tail-to-tail.

Forming of open edges in lipid membranes results in exposer of the tail groups at the edge to water [4], which is energetically unfavourable. As a result, phospholipid molecules rapidly rearrange around the exposed edge, forming a semicylindrical rim along it. This rearrangement is the source of a line energy at the edge. In order to eliminate this edge energy, lipid bilayers commonly tend to form closed structures such as spheroids [7]. Nevertheless, they can transiently open due to various stimuli such as mechanical stresses and thermal instabilities. The formation of these transient pores is essential for regulation of PH, transmembrane electrochemical potential, and concentrations of different molecules in the cell [5]. Additionally, transient open membranes are formed during electro-formation [8]. More recently, stabilizing pores and control over their size have been pursued by means of electric fields [9], sonication [10], and use of edge-active chemical agents [11]. The rapid progress in these techniques has attracted increasing attention to the study of the open lipid bilayers, including molecular dynamic simulations, as well as continuum mechanical treatment and numerical investigations of the equilibrium configurations [12, 13].

Theoretical studies of the equilibrium and stability of pored membranes have mainly relied on constitutive assumptions for the edge, which neglect its flexural and torsional elasticity. For instance, Boal and Rao [14], Capovilla *et al.* [15], and Tu and Ou-Yang [16, 17] considered the edge energy of an open lipid bilayer as a given constant. Tu and Ou-Yang [18] considered dependence of the edge energy on its geometry, namely geodesic and normal curvatures. Nevertheless, their assumptions on the form of the line energy have not been precisely justified.

May [19] obtained the line energy of a lipid bilayer edge through optimization of the lipid packing at the vicinity of the edge. He modeled the edge as a semicylindrical micelle, and took the free energy per molecule to depend upon the chain length of the molecules, their cross-sectional area, and the strength of the interactions of the molecules with each other and with the surrounding solution. Although successful in obtaining the line tension, that framework did not capture the bending and torsional energetics of the edge. The gap in the literature to successfully relate the macro-scale edge energy to its microstructure has motivated the current study.

The interactions between the constituent molecules of a material may be used to obtain the free-energy density function of that material. For instance, Keller and Merchant [20] have employed such a microphysical approach to extract the internal energy, surface tension, and bending energy of a liquid surface and to relate its bending rigidity to the molecular density and interaction potential. In a recent application of the work of Keller and Merchant [20], the Canham–Helfrich free-energy density for a lipid vesicle was derived based on microphysical considerations [21]. Using the same approach, a model for the elastic free-energy of wormlike micelles was derived [22]. In so doing, the surfactant molecules comprising the wormlike micelle were assumed to have constant length, and thus, were

modeled by one-dimensional rigid rods. The resulted expression for the free energy was found to be quadratic in the curvature and torsion of the centerline of the micelle [22].

The current study adopts the microphysical approach of Keller and Merchant [20] to investigate the elastic behaviour of the edge of a lipid bilayer. Following May [19] and motivated by previous studies [23, 24, 25, 26], the edge is modeled as a semicylindrical surface. In addition, the phospholipid molecules comprising the edge are modeled as one-dimensional rigid rods of constant length, oriented perpendicular to the centerline of the edge. The applied framework enables us to extract the form of the free energy and the flexural and torsional moduli of the edge, based on the intermolecular energetic interaction between phospholipid molecules.

To find the free-energy density of the edge at a position $\boldsymbol{x}$, we account for the interactions between all phospholipid molecules on the edge within a cutoff distance δ from the molecules at $\boldsymbol{x}$. We assume that the phospholipid molecules are perpendicular to the centerline of the edge. Our derivation relies on Taylor series expansions with respect to a dimensionless parameter $\varrho := \delta/\ell \ll 1$, where ℓ is a characteristic size parameter of the edge, such as its length. For ℓ taken as the length of the edge (or equivalently, the perimeter of a pore), it can be related to the thickness or the length of the constituent molecules, if the density of the molecules along the edge and their aspect ratios are provided. The net free-energy of the edge results from integrating the free-energy density φ over the centerline of the edge.

The paper is structured as follows. In Section 2, required mathematical definitions are presented. Modeling assumptions for the edge of an open lipid bilayer are synopsized in Section 3. Section 4 is concerned with the derivation of the free-energy density of such an edge. In Section 5, the consequences of choosing a spheroidal-particle potential (Berne and Pechukas [27] and Gay and Berne [28]) are considered to obtain the material parameters present in the derived model. As an illustrative example, a simplified model for a pore on a lipid bilayer is given in Section 6, and the parameters obtained in Section 5 are used to find the free-energy of the pore as a function of its size. Finally, the key findings of the study are summarized and discussed in Section 7. Details of the various derivations are provided in the Appendix.

2. Differential geometry of the bounding curve of a surface

Consider a smooth, orientable, open surface $\mathscr{S}$ representing the open lipid bilayer, with boundary $\mathscr{C}=\partial\mathscr{S}$, as depicted schematically in Figure 1. Let

$$\mathscr{C}=\{\boldsymbol{x}:\boldsymbol{x}=\boldsymbol{x}(s),\quad 0\leq s\leq L\},\quad (1)$$

denote the arclength parametrization of the closed boundary curve $\mathscr{C}$. On denoting the differentiation with respect to the arclength s by a superposed dot, it follows that $|\dot{\boldsymbol{x}}|=1$, and thus,

$$\dot{\boldsymbol{x}}\cdot\ddot{\boldsymbol{x}}=0,\quad \text{and}\quad |\dot{\boldsymbol{x}}\times\ddot{\boldsymbol{x}}|=|\ddot{\boldsymbol{x}}|.\quad (2)$$

The unit tangent of $\mathscr{C}$ is introduced, in terms of the arclength parametrization $\boldsymbol{x}$, by

$$\mathbf{t} := \dot{\boldsymbol{x}} . \quad (3)$$

Since the unit tangent **t** has a constant length, its arclength derivative $\dot{\mathbf{t}} = \mathrm{d}\mathbf{t}/\mathrm{d}s$ is perpendicular to it, and thus, perpendicular to the curve $\mathscr{C}$. The orientation of $\dot{\mathbf{t}}$ is called the unit normal of $\mathscr{C}$, and is denoted by **N**. The curvature vector $\boldsymbol{\kappa}$ at any point of $\mathscr{C}$ is then defined by the arclength derivative of the unit tangent **t** as

$$\boldsymbol{\kappa} := \dot{\mathbf{t}} = \kappa \mathbf{N}, \quad (4)$$

where κ denotes the magnitude of the curvature of $\mathscr{C}$ at that point, which is given in terms of the arclength parametrization $\boldsymbol{x}$, by

$$\kappa = |\dot{\boldsymbol{x}} \times \ddot{\boldsymbol{x}}| = |\ddot{\boldsymbol{x}}|. \quad (5)$$

For an arbitrary point on curve $\mathscr{C}$ at which $\kappa \neq 0$, the unit binormal vector is defined by **B** = **t** × **N**. The unit tangent **t**, unit normal **N**, and unit binormal **B** at each point of $\mathscr{C}$, form the Frenet frame {**t**, **N**, **B**} at that point.

The torsion τ of $\mathscr{C}$ is defined by $\dot{\mathbf{B}} = -\tau \mathbf{N}$, and is expressed in terms of the arclength parametrization $\boldsymbol{x}$ as

$$\tau = \frac{\dot{\boldsymbol{x}} \cdot \left(\ddot{\boldsymbol{x}} \times \dddot{\boldsymbol{x}} \right)}{|\ddot{\boldsymbol{x}}|^2}. \quad (6)$$

The torsion τ of $\mathscr{C}$, describes the tendency of the curve $\mathscr{C}$ to move out of its osculating plane at a given point, or, equivalently, it measures the turnaround of the unit binormal **B** of $\mathscr{C}$ at a given point. In general, a space curve is determined up to a rigid translation, by its two locally invariant quantities: the curvature κ and torsion τ, both in terms of the arclength parameter σ.

On the boundary curve $\mathscr{C}$ of the surface $\mathscr{S}$, the unit normal to the surface is denoted by $\boldsymbol{n}$. Also, since $\dot{\boldsymbol{x}}$ is a unimodular vector, its arclength derivative $\ddot{\boldsymbol{x}}$ is perpendicular to $\dot{\boldsymbol{x}}$, and thus, can be considered as a linear combination

$$\ddot{\boldsymbol{x}} = \kappa_n \boldsymbol{n} + \kappa_g \quad \boldsymbol{n} \times \dot{\boldsymbol{x}}, \quad (7)$$

of the unit normal $\boldsymbol{n}$, and the product $\boldsymbol{n} \times \dot{\boldsymbol{x}}$. Notice that the unit normal $\boldsymbol{n}$ to the surface $\mathscr{S}$ is different from the unit normal **N** of the curve $\mathscr{C}$. Further, let $\boldsymbol{p}$ denote the unit vector in the tangent plane of $\mathscr{S}$ perpendicular to the unit tangent $\boldsymbol{t}$ while pointing outward. We call $\boldsymbol{p}$ the unit tangent-normal. The set of unit normal $\boldsymbol{n}$ to the surface $\mathscr{S}$ at $\mathscr{C}$, unit tangent-normal $\boldsymbol{p}$, and the unit tangent $\boldsymbol{t}$, which is $\boldsymbol{t} = \boldsymbol{n} \times \boldsymbol{p}$, form the oriented basis {$\boldsymbol{t}$, $\boldsymbol{n}$, $\boldsymbol{p}$} on $\mathscr{C}$, known as the Darboux frame (Figure 1). Considering that the normal **N** and binormal **B** of the Frenet frame of $\mathscr{C}$ are also perpendicular to $\boldsymbol{t}$, they both lie in the plane spanned by the normal $\boldsymbol{n}$ and tangent-normal $\boldsymbol{p}$ of the Darboux frame. Therefore, they are related to $\boldsymbol{n}$ and $\boldsymbol{p}$ by

$$\left.\begin{aligned}\mathbf{N}&=(cos\,\psi)\,\boldsymbol{n}-(sin\,\psi)\,\boldsymbol{p},\\ \mathbf{B}&=(sin\,\psi)\,\boldsymbol{n}+(cos\,\psi)\,p,\end{aligned}\right\} \quad (8)$$

where ψ denotes the angle between the unit normal **N** of the curve $\mathscr{C}$ and the unit normal ***n*** to the surface $\mathscr{S}$. Following the proof provided in Appendix A, derivatives of ***t***, ***n***, and ***p*** with respect to the arclength *s* along $\mathscr{C}$ are expressed as

$$\begin{bmatrix}\dot{\boldsymbol{t}}\\ \dot{\boldsymbol{n}}\\ \dot{\boldsymbol{p}}\end{bmatrix}=\begin{bmatrix}0 & \kappa\,cos\,\psi & -\kappa\,sin\,\psi\\ -\kappa\,cos\,\psi & 0 & \tau+\dot{\psi}\\ \kappa\,sin\,\psi & -\tau-\dot{\psi} & 0\end{bmatrix}\begin{bmatrix}\boldsymbol{t}\\ \boldsymbol{n}\\ \boldsymbol{p}\end{bmatrix}. \quad (9)$$

The quantity

$$\tau_g=\tau+\dot{\psi}, \quad (10)$$

is called *geodesic torsion* of the curve $\mathscr{C}$ on $\mathscr{S}$. This quantity describes the rate of the rotation of the tangent plane of the surface $\mathscr{S}$ about the unit tangent to the curve $\mathscr{C}$ with respect to the arc length *s* [29]. Also, τ_g can be expressed alternatively as

$$\tau_g=\dot{\boldsymbol{x}}\cdot(\boldsymbol{n}\times\dot{\boldsymbol{n}}). \quad (11)$$

Further, the curvature vector $\boldsymbol{\kappa}$ of the curve $\mathscr{C}$ on the surface $\mathscr{S}$ is the sum of the normal curvature vector $\boldsymbol{\kappa_n}$, and the tangential (or geodesic) curvature vector $\boldsymbol{\kappa_g}$, i.e.

$$\boldsymbol{\kappa}=\boldsymbol{\kappa_n}+\boldsymbol{\kappa_g}. \quad (12)$$

The normal curvature vector $\boldsymbol{\kappa_n}$ is the projection of the curvature vector $\boldsymbol{\kappa}$ along the normal ***n*** of the surface $\mathscr{S}$. The geodesic curvature $\boldsymbol{\kappa_g}$ is perpendicular to the unit normal ***n*** to the surface, and, thus, lies in the tangent plane of the surface $\mathscr{S}$. Hence,

$$\boldsymbol{\kappa_n}=(\boldsymbol{\kappa}\cdot\boldsymbol{n})\,\boldsymbol{n}, \quad \text{and} \quad \boldsymbol{\kappa_g}=\boldsymbol{n}\times(\boldsymbol{\kappa}\times\boldsymbol{n}). \quad (13)$$

According to (4), the curvature vector $\boldsymbol{\kappa}$ of $\mathscr{C}$ is $\boldsymbol{\kappa}=\kappa\mathbf{N}$. Since ψ denotes the angle between **N** and ***n***, the magnitude κ_n of the normal curvature $\boldsymbol{\kappa_n}$ is

$$\kappa_n=\boldsymbol{\kappa}\cdot\boldsymbol{n}=\kappa\,\mathbf{N}\cdot\boldsymbol{n}=\kappa\,\mathbf{cos}\,\psi. \quad (14)$$

The magnitude κ_g of the tangential (or geodesic) curvature vector $\boldsymbol{\kappa_g}$, is a bending invariant, and is given by

$$\kappa_g=-\boldsymbol{p}\cdot\dot{\boldsymbol{t}}=-\kappa\,\boldsymbol{p}\cdot\mathbf{N}=(\boldsymbol{n}\times\boldsymbol{t})\cdot\dot{\boldsymbol{t}}. \quad (15)$$

According to $\dot{\boldsymbol{t}}=\kappa\mathbf{N}$, and

$$\boldsymbol{n}=(cos\,\psi)\,\mathbf{N}+(sin\,\psi)\,\mathbf{B}, \quad (16)$$

the right-hand side of (15) results

$$\boldsymbol{\kappa_g}=\kappa_g\,(\boldsymbol{n}\times\boldsymbol{t})\,,\quad \text{where}\,\kappa_g=\kappa\,sin\,\psi. \quad (17)$$

As mentioned earlier, the geodesic curvature vector $\boldsymbol{\kappa_g}$ at any point of the curve $\mathscr{C}$ on the surface $\mathscr{S}$ is the vectorial projection of the curvature vector $\boldsymbol{\kappa}$ of the curve $\mathscr{C}$ into the tangent plane of the surface $\mathscr{S}$ at that point. This quantity is an intrinsic property of the surface, which reflects the deviation of the curve $\mathscr{C}$ from a geodesic on the surface $\mathscr{S}$ [30]. In general, for a geodesic, the geodesic curvature κ_g at any point is zero. Further, for a geodesic, the unit normal **N** of the curve $\mathscr{C}$ coincides with the unit normal $\boldsymbol{n}$ of the surface $\mathscr{S}$, or, equivalently, the osculating plane of $\mathscr{C}$ at each point is perpendicular to the tangent plane of the surface $\mathscr{S}$ at that point [29]. This means that the Darboux frame and the Frenet frame for a geodesic are the same at any point.

According to (10), and the right-hand sides of (14) and (17), the arclength derivatives of {$\boldsymbol{t}$, $\boldsymbol{n}$, $\boldsymbol{p}$} in (9) take the form

$$\left.\begin{aligned}\dot{\boldsymbol{t}}&=\kappa_n\boldsymbol{n}-\kappa_g\boldsymbol{p},\\ \dot{\boldsymbol{n}}&=-\kappa_n\boldsymbol{t}+\tau_g\boldsymbol{p},\\ \dot{\boldsymbol{p}}&=\kappa_g\boldsymbol{t}-\tau_g\boldsymbol{n}.\end{aligned}\right\} \quad (18)$$

3. Modeling assumptions

The phospholipid molecules comprising the edge are allocated so that their hydrophilic parts lie on a thin semicylindrical surface as shown in Figure 2 to form a core shielding the hydrophobic tails from the surrounding solution. The centerline of the edge is denoted by a boundary curve $\mathscr{C}$. The following assumptions, which are based on the previously reported observations [23, 24, 26, 31, 32], are considered to model the edge of an open lipid bilayer:

(i) · The phospholipid molecules comprising the edge are modeled as one-dimensional rigid rods of the same length *a*.

(ii) · The lipid molecules are assumed to be perpendicular to the centerline $\mathscr{C}$, residing in the plane spanned by the unit normal **n** and the unit tangent-normal **p**, as depicted in Figure 2. This assumption is valid as long as the concentration of the lipid molecules on the edge $\mathscr{C}$ is sufficiently high.

(iii) · The phospholipid molecules at any cross-section of the edge have uniform angular distribution.

(iv) · The distribution of the phospholipid molecules at any point along $\mathscr{C}$ is denoted by the molecular density function $\Pi > 0$. In contrast to the angular distribution, which is assumed to be uniform because of symmetry considerations, the molecular distribution along $\mathscr{C}$ may be nonuniform as a result of localized curvature.

Consider a lipid molecule at the position corresponding to *s* on $\mathscr{C}$ with orientation θ measured counterclockwise from the corresponding tangent-normal $\boldsymbol{p}(s)$, as depicted

schematically in Figure 2b. Let the director $\boldsymbol{d}(s, \theta)$ denote the orientation of this molecule. By the second assumption, such a director can be expressed as a linear combination

$$\boldsymbol{d}(s,\theta) = (cos\,\theta)\ \boldsymbol{p}(s) + (sin\,\theta)\ \boldsymbol{n}(s), \quad (19)$$

where $\boldsymbol{p}(s)$ and $\boldsymbol{n}(s)$ denote the tangent-normal and the unit normal (to $\mathscr{S}$) at the position corresponding to s.

4. Derivation of the free-energy density

In this section, the free-energy density of the edge of an open lipid bilayer is derived taking into account the interactions between the molecules comprising the edge. To do so, a microphysical approach is applied, guided by the work of Keller and Merchant [20].

Consider two molecules, with directors $\boldsymbol{d}$ and $\boldsymbol{d}'$, located respectively at positions $\boldsymbol{x}$ and $\boldsymbol{x}'$ interior to $\mathscr{C}$. Let the interaction energy (encompassing steric, electrostatic, and other relevant effects) between the molecules under consideration be denoted by

$$\Omega\left(\boldsymbol{x}, \boldsymbol{x}', \boldsymbol{d}, \boldsymbol{d}'\right). \quad (20)$$

Following Keller and Merchant [20], we assume that the interaction energy between two molecules separated by more than a fixed cutoff distance δ vanishes, in which case

$$\Omega\left(\boldsymbol{x}, \boldsymbol{x}', \boldsymbol{d}, \boldsymbol{d}'\right) = 0 \quad \text{if} \quad |\boldsymbol{x} - \boldsymbol{x}'| > \delta. \quad (21)$$

In the present setting, the cutoff distance δ is required to be small relative to the characteristic length ℓ of the edge, so that a dimensionless measure ϱ of cutoff distance obeys

$$\varrho := \frac{\delta}{\ell} \ll 1. \quad (22)$$

Hereafter, we restrict attention to interaction energies Ω that are of the form (20) but are also frame indifferent [33]. It then follows that $\Omega(\boldsymbol{x}, \boldsymbol{x}', \boldsymbol{d}, \boldsymbol{d}')$ may depend on the positions $\boldsymbol{x}$ and $\boldsymbol{x}'$ and the directors $\boldsymbol{d}$ and $\boldsymbol{d}'$ only through the length $|\boldsymbol{x}-\boldsymbol{x}'|$ of the vector between $\boldsymbol{x}$ and $\boldsymbol{x}'$, the dot products $(\boldsymbol{x}-\boldsymbol{x}')\cdot\boldsymbol{d}$ and $(\boldsymbol{x}-\boldsymbol{x}')\cdot\boldsymbol{d}'$ formed by the directors and that vector, and the dot product $\boldsymbol{d}\cdot\boldsymbol{d}'$ formed by the directors. Like Keller and Merchant [20], we assume that dependence of the interaction energy on the length of the relative position vector is scaled by the ratio ϱ defined in (22) and, thus, that

$$\Omega\left(\boldsymbol{x}, \boldsymbol{x}', \boldsymbol{d}, \boldsymbol{d}'\right) = 2\tilde{\Omega}\left(\varrho^{-2}\boldsymbol{r}\cdot\boldsymbol{r}, \boldsymbol{r}\cdot\boldsymbol{d}, \boldsymbol{r}\cdot\boldsymbol{d}', \boldsymbol{d}\cdot\boldsymbol{d}'\right), \quad (23)$$

with $\boldsymbol{r} = \boldsymbol{x} - \boldsymbol{x}'$. The factor of two in the right-hand side of (23) is for simplifying later calculations. Notice that Ω depends explicitly on δ, whereas $\tilde{\Omega}$ does not. Consequently, (21), (22), and (23) yield

$$\tilde{\Omega}\left(s^2,\rho_1,\rho_2,\rho_3\right)=0 \quad \text{if} \quad s>\ell, \quad (24)$$

where

$$\rho_1=s\varrho\,\hat{\boldsymbol{r}}\cdot\boldsymbol{d}, \quad \rho_2=s\varrho\,\hat{\boldsymbol{r}}\cdot\boldsymbol{d}', \quad \rho_3=s\varrho\,\boldsymbol{d}\cdot\boldsymbol{d}', \quad (25)$$

with $\hat{\boldsymbol{r}}$ being the unit vector corresponding to the intermolecular vector $\boldsymbol{r}$.

As a consequence of the foregoing discussion, the net free-energy φ_{net} of the edge can be expressed as

$$\phi_{net}=\int_0^L \frac{1}{2}\left(\int_{-\frac{\pi}{2}}^{\frac{\pi}{2}}\omega\left(s,\theta\right)\,\mathrm{d}\theta\right)\Pi\left(s\right)\,\mathrm{d}s, \quad (26)$$

where

$$\omega\left(s,\theta\right)=\int_0^L\int_{\frac{-\pi}{2}}^{\frac{\pi}{2}}\Omega\left(\boldsymbol{x}\left(s\right),\boldsymbol{x}\left(t\right),\boldsymbol{d}\left(s,\theta\right),\boldsymbol{d}\left(t,\eta\right)\right)\Pi\left(t\right)\,\mathrm{d}\eta\,\mathrm{d}t \quad (27)$$

is the free energy due to the interactions between the molecule with director $\boldsymbol{d}(s,\theta)$ at $\boldsymbol{x}(s)$ with all other molecules and where a factor of one-half compensates for the double counting of interactions arising from integrating over both s and t from 0 to L. From (26), the free-energy density φ at position $\boldsymbol{x}(s)$ on $\mathscr{C}$ is simply

$$\phi=\frac{1}{2}\left(\int_{\frac{-\pi}{2}}^{\frac{\pi}{2}}\omega\left(s,\theta\right)\,\mathrm{d}\theta\right)\Pi\left(s\right). \quad (28)$$

The function Π denotes the density of the lipid molecules at any point of the curve $\mathscr{C}$. Following the proof which relies on the Taylor series expansion of the integrand of (28) with respect to ϱ up to the second derivative term, provided in Appendix B, (28) becomes

$$\phi=k_\circ+k_1\kappa_g^2+k_2\kappa_n^2+k_3\kappa_g+k_4\kappa_n+k_5\kappa_n\kappa_g+k_6\tau_g^2, \quad (29)$$

which includes a quadratic expression in terms of κ_g, κ_n, and τ_g. Also, $k_\bigcirc$ and the coefficients k_i in (29) are provided in Appendix B. Notice that $k_\bigcirc$ is the standard line energy of the edge—the part which is independent of edge geometry—while the coefficients k_i, i = 1, 2, 5, 6 represent the flexural and torsional rigidities of the edge. Up to the second derivative term of the Taylor expansion considered here, the derived model (29) contains the linear terms of the normal curvature κ_n and the geodesic curvature κ_g of the boundary curve $\mathscr{C}$, while it does not incorporate the linear term of the geodesic torsion τ_g of $\mathscr{C}$. Considering a simplification of (29) in the form

$$\phi=\bar{k}_\circ+k_1(\kappa_g-\kappa_{g\circ})^2+k_2(\kappa_n-\kappa_{n\circ})^2+k_5\kappa_n\kappa_g+k_6{\tau_g}^2, \quad (30)$$

where

$$\kappa_{g\circ}=-\frac{k_3}{2k_1},\quad \kappa_{n\circ}=-\frac{k_4}{2k_2},\quad \bar{k}_{\circ}=k_{\circ}-\frac{k_3^2}{4k_1}-\frac{k_4^2}{4k_2},\quad (31)$$

it can be inferred that the remaining coefficients k_3 and k_4 are related to the spontaneous geodesic and normal curvatures $\kappa_{g\bigcirc}$ and $\kappa_{n\bigcirc}$ of $\mathscr{C}$. This transpires that our model captures the spontaneous normal and geodesic curvatures $\kappa_{n\bigcirc}$ and $\kappa_{g\bigcirc}$ of the edge, while an spontaneous geodesic torsion is absent from the free energy. Further, (29) and (30) include the coupling of the normal curvature κ_n and the geodesic curvature κ_g via the term $\kappa_n\kappa_g$. However, the couplings of the geodesic torsion τ_g with the normal and geodesic curvatures κ_n and κ_g are absent. Our calculations show that the latter terms only appear by including higher order terms in the Taylor expansion, and hence, are of less significance. In addition, if the molecules have non-uniform angular distribution, i.e. the molecular distribution function Π is allowed to depend upon θ or η, the model would also include a linear term in geodesic torsion τ_g that would lead to the presence of a spontaneous geodesic torsion.

The first term $k_{\bigcirc}$ on the right-hand side of (30) is insensitive to the shape of the boundary. Since the molecular distribution on the boundary has implicit dependence upon the ambient temperature and concentration, these effects may be encompassed in $k_{\bigcirc}$ and in the moduli k_1–k_6. The line tension $k_{\bigcirc}$ has been obtained through experiments and molecular dynamic simulations for various types of lipid bilayers (see [23] for a comparison of different measurements). However, there is not enough literature on measurement of the remaining coefficients. By fitting our model to existing measurements of the line tension, the controlling parameters of the interaction potential can be evaluated, and further used to obtain the remaining coefficients in (29).

The derived model (29) can be simplified into the previously presented models for the free-energy of the edge. In particular, the general form (29) provides a development to the theoretical investigations of open lipid bilayers presented by Tu and Ou-Yang [12], and Guven *et al.* [31].

4.1. Total free-energy of the edge

The net free-energy φ_{net} associated with the elasticity of the edge of the open lipid bilayer is simply obtained by integrating the free-energy density φ in (30) over the centerline $\mathscr{C}$ of the edge by

$$\phi_{net}=\int_0^L \phi\,\mathrm{d}s.\quad (32)$$

5. Applying a concrete interaction potential

The interaction potential in the model developed in the previous section was assumed to be a general function of four frame-indifferent arguments in terms of the intermolecular vector and the orientation of phospholipid molecules. There are numerous concrete models for such interaction potentials between axisymmetric particles, which are vastly employed for numerical simulations of liquid crystals and other similar systems. Our derivation gives rise to integral representations for elastic moduli $k_{\bigcirc}$–k_6 of the edge. Substituting the general

form $\tilde{\Omega}$ in (B.1) with an available interaction potential yields the material parameters $k_{\bigcirc}$–k_6 appearing in (29).

One of the standard examples among such pair interaction potentials is the spheroidal-particle model proposed by Berne and Pechukas [27], and Gay and Berne [28], in which the molecules are approximated by ellipsoids of revolution, or spheroids (see Figure 3). According to such model, the interaction potential between two molecules with the intermolecular vector $\boldsymbol{r}$ and the directors $\boldsymbol{d}$ and $\boldsymbol{e}$ possesses the multiplicative decomposition

$$\tilde{\Omega}(\boldsymbol{r},\boldsymbol{d},\boldsymbol{e}) = \xi(\hat{\boldsymbol{r}},\boldsymbol{d},\boldsymbol{e})\,\zeta(\boldsymbol{r},\boldsymbol{d},\boldsymbol{e}), \quad (33)$$

where $\xi(\hat{\boldsymbol{r}},\boldsymbol{d},\boldsymbol{e})$ and $\zeta(\boldsymbol{r},\boldsymbol{d},\boldsymbol{e})$ denote the strength and distance parameters respectively. The strength parameter $\xi(\hat{\boldsymbol{r}},\boldsymbol{d},\boldsymbol{e})$ depends upon the orientation of the molecules and that of the intermolecular vector $\boldsymbol{r}$ through (Gay and Berne [28])

$$\xi(\hat{\boldsymbol{r}},\boldsymbol{d},\boldsymbol{e}) = \frac{4\,\xi_{\circ}}{\left(1-\chi^2(\boldsymbol{d}\cdot\boldsymbol{e})^2\right)^{\nu/2}}\left[1-\frac{\chi'}{2}\left(\frac{(\hat{\boldsymbol{r}}\cdot\boldsymbol{d}+\hat{\boldsymbol{r}}\cdot\boldsymbol{e})^2}{1+\chi'\boldsymbol{d}\cdot\boldsymbol{e}}+\frac{(\hat{\boldsymbol{r}}\cdot\boldsymbol{d}-\hat{\boldsymbol{r}}\cdot\boldsymbol{e})^2}{1-\chi'\boldsymbol{d}\cdot\boldsymbol{e}}\right)\right]^{\mu}, \quad (34)$$

with ν, μ, and $\xi_{\bigcirc}$ the fitting parameters to be chosen. More specifically, ν depends upon the arrangement type of the molecules (e.g. side-to-side or end-to-end), whereas $\xi_{\bigcirc}$ is a constant that specifies the kind of molecules under consideration. The parameter χ in (34) is the shape anisotropy parameter, given in terms of the ratio of the length σ_e to the breadth σ_s of the molecules by

$$\chi = \frac{(\sigma_e/\sigma_s)^2-1}{(\sigma_e/\sigma_s)^2+1}. \quad (35)$$

Also, the parameter χ' in (34) is given by

$$\chi' = \frac{(\varepsilon_e/\varepsilon_s)^{1/\mu}-1}{(\varepsilon_e/\varepsilon_s)^{1/\mu}+1}, \quad (36)$$

where ε_e and ε_s denote the strength parameters for end-to-end and side-to-side arrangement of the molecules respectively. The distance parameter $\zeta(\boldsymbol{r},\boldsymbol{d},\boldsymbol{e})$ in (33) is given by (Berne and Pechukas [27])

$$\zeta(\boldsymbol{r},\boldsymbol{d},\boldsymbol{e}) = exp\left(\frac{-|\boldsymbol{r}|^2}{\varsigma^2(\hat{\boldsymbol{r}},\boldsymbol{d},\boldsymbol{e})}\right), \quad (37)$$

where $\varsigma(\hat{\boldsymbol{r}},\boldsymbol{d},\boldsymbol{e})$ is called the range parameter and is given as a function of the orientation of the molecules and that of the intermolecular vector **r** by

$$\varsigma(\hat{r},\boldsymbol{d},\boldsymbol{e}) = \sigma_{\circ}\left[1-\frac{\chi}{2}\left(\frac{(\hat{\boldsymbol{r}}\cdot\boldsymbol{d}+\hat{\boldsymbol{r}}\cdot\boldsymbol{e})^2}{1+\chi\boldsymbol{d}\cdot\boldsymbol{e}}+\frac{(\hat{\boldsymbol{r}}\cdot\boldsymbol{d}-\hat{\boldsymbol{r}}\cdot\boldsymbol{e})^2}{1-\chi\boldsymbol{d}\cdot\boldsymbol{e}}\right)\right]^{\frac{-1}{2}}. \quad (38)$$

In (38), $\sigma_{\bigcirc}$ is related to the breadth of the molecules, σ_s, via $\sigma_{\bigcirc} = \sqrt{2}\sigma_s$. Following Whitehead *et al.* [34], the parameters μ and ν are chosen as

$$\nu = -1, \quad \text{and} \quad \mu = 2. \quad (39)$$

By applying the interaction potential (33) in (B.7), and assuming a constant molecular density Π along the boundary $\mathscr{C}$, the coefficients k_i in (29) are obtained as

$$\begin{aligned} &\frac{k_\circ}{\Pi^2 \xi_\circ \sigma_\circ} = \sqrt{\pi}\, erf\,(x)\, I_\circ, \\ &\frac{k_1}{\Pi^2 \xi_\circ \sigma_\circ^3} = \frac{k_2}{\Pi^2 \xi_\circ \sigma_\circ^3} = \frac{\sqrt{\pi}}{128} erf\,(x)\left(\chi^2 J + \left(\chi^2+2\right) I\right) + \frac{x e^{-x^2}}{192}\left(\chi^2 (J+I)\left(2x^2-3\right) - 2I\left(2x^2+3\right)\right), \\ &k_3 = k_4 = k_5 = k_6 = 0. \end{aligned} \quad (40)$$

where x is a dimensionless parameter defined as the ratio of the cut-off distance δ to $\sigma_{\bigcirc}$ as

$$x = \frac{\delta}{\sigma_\circ}, \quad (41)$$

and $I_{\bigcirc}$, I and J are integral representations shown in Appendix C. Hence, the free-energy density φ in (29) specializes to

$$\phi = k_\circ + k_1\left(\kappa_n^2 + \kappa_n^2\right) = k_\circ + k_1\,\kappa^2. \quad (42)$$

A single phospholipid molecule can be envisioned as a molecule in which a water-soluble spherical head is attached to a pair of water-insoluble tails. Here we rely on the dimensions of a specific kind of phospholipid molecule (DPPC/Water system) reported by Mashaghi *et al.* [35] According to their estimation, the length of the aforementioned phospholipid molecule from the center of the head-group to the tail is ~ 22.5–30 $A^{\bigcirc}$, and the diameter of the head-group is ~ 7–10 $A^{\bigcirc}$. The total volume of that molecule is thus the sum of the volume of the spherical head and that of a cylindrical tail-group. Based on the equality of the volumes of the phospholipid molecule and that of the spheroidal replacement, the aspect ratio σ_e/σ_s of the spheroid in Figure 3 is obtained between 3 and 4. Hence, the schematic of the constant line energy $k_{\bigcirc}$ and that of the flexural rigidity k_1 are depicted in terms of the dimensionless cutoff distance $\delta/\sigma_{\bigcirc}$ in Figure 4, for molecular aspect ratio σ_e/σ_s between 1 and 5. According to Figure 4, the change in the constant line energy $k_{\bigcirc}$ and flexural rigidity k_1 is negligible after some value of the dimensionless cutoff distance $\delta/\sigma_{\bigcirc}$. Therefore, a rather conservative choice for the cut-off distance, which guarantees inclusion of all significant molecular interactions, is

$$\delta^* = 3\sigma_\circ. \quad (43)$$

This result has been used to obtain the constant part of the line energy $k_{\bigcirc}$ and flexural rigidity k_1 of the edge in terms of the molecular aspect ratio, as depicted in Figure 5.

6. Illustrative example: dependence of free-energy on the pore size

In order to estimate the change of energy of a pore with its size, consider the simple case of a spherical lipid bilayer with radius R, with a pore of radius r at a distance h from its centre, as depicted in Figure 6. For such a pore, the total curvature of the boundary curve $\mathscr{C}$ is $1/r$, and the geodesic torsion τ_g vanishes. Also, the normal and geodesic curvatures find the froms

$$\kappa_n=\frac{1}{R},\quad \text{and}\quad \kappa_g=\sqrt{\kappa^2-\kappa_n^2}=\frac{\sqrt{R^2-r^2}}{rR}. \quad (44)$$

As a result, the free-energy density (30) specializes to

$$\phi=k_\circ+k_1\left(\frac{\sqrt{R^2-r^2}}{rR}-\kappa_{g\circ}\right)^2+k_2\left(\frac{1}{R}-\kappa_{n\circ}\right)^2+k_5\left(\frac{\sqrt{R^2-r^2}}{rR^2}\right), \quad (45)$$

which with (32), yields a representation for the net free-energy φ_{net} of the pore as

$$\frac{\phi_{net}}{2\pi r}=k_\circ+k_1\left(\frac{\sqrt{R^2-r^2}}{rR}-\kappa_{g\circ}\right)^2+k_2\left(\frac{1}{R}-\kappa_{n\circ}\right)^2+k_5\left(\frac{\sqrt{R^2-r^2}}{rR^2}\right). \quad (46)$$

It was demonstrated in the previous section that when the spheroidal interaction potential [27] is employed in the microphysical model, the spontaneous curvatures $\kappa_{g\bigcirc}$ and $\kappa_{n\bigcirc}$, and the coefficient k_5 vanish, while the bending moduli k_1 and k_2 find the same value. Using those results in (46) yields

$$\frac{\phi_{net}}{2\pi}=k_\circ r+\frac{k_1}{r}, \quad (47)$$

whereby the energy of the pore does not depend on the size of the lipid bilayer, nor on the placing of the pore on it. For the cut-off distance $\delta^* = 3\sigma_\bigcirc$ and the molecular aspect ratios $\sigma_e/\sigma_s = 3$ and $\sigma_e/\sigma_s = 4$, the dependence of the net free-energy to pore size has been demonstrated in Figure 7. The second term in the right-hand side of (47) leads to a minimum point for the free energy for $r < \sigma_\bigcirc$, which does not fall in the physically-relevant ranges of the pore size. For reasonable values of $r/\sigma_\bigcirc$, the first term on the right of (47) is dominant and the dependence of the net energy on the pore size is effectively linear.

7. Discussion and Summary

An expression for the free-energy density of the edge of an open lipid bilayer was derived taking into account the interaction between the constituent molecules. The resulting expression contains quadratic terms in geodesic curvature, normal curvature, and geodesic torsion of the boundary curve and a term including the multiplication of geodesic and normal curvatures. The derived free-energy of the edge is the evidence of an excess energy due to the specific arrangement of the phospholipid molecules in the vicinity of the boundary of an open bilayer, in accord with the results of the existing molecular dynamic simulations [23, 24, 25, 26]. Further, our study supplements the previous molecular dynamic

simulations [23, 24, 25, 26] and theories [19] in which the free energy was obtained as a constant, by providing the contribution due to bending and torsional energies. For certain classes of lipid bilayers, the bending free-energy, which can be captured by our framework, is of more importance in contrast to the line energy [36, 37]. In addition, our microphysical model justifies the constitutive assumptions that appear in continuum mechanical theories for open lipid bilayers [12, 38, 31].

Our derivation gives rise to integral representations for the material parameters present in the model. Specifically, the molecular origins of the spontaneous curvatures of the edge of a lipid bilayer have been investigated. A concrete soft-core interaction potential for axisymmetric rod-like molecules was applied on the derived model to obtain those material parameters. Hence, a special form of the interaction potential suggested by Berne and Pechukas [27] was employed to further explore the developed microphysical model. Assuming that the molecules are uniformly distributed along the edge, (i.e.Π =constant), the spontaneous curvatures and the torsional contribution to the energy vanish, resulting in (42), which includes only a constant part $k_{\bigcirc}$, which can be interpreted as a line tension, and a contribution due to bending with flexural rigidity $k_1 = k_2$. The dependence of the parameters $k_{\bigcirc}$ and k_1 on the aspect ratio σ_e/σ_s and the dimensionless cutoff distance $\delta/\sigma_{\bigcirc}$, for various aspect ratios common for phospholipid molecules comprising lipid membranes, was investigated. It was concluded that increasing the cut-off distance after a value $\delta^* = 3\sigma_{\bigcirc}$ does not affect those parameters. This result and the definition $\sigma_{\bigcirc} = \sqrt{2}\sigma_s$ reveals that each molecule on the edge interacts with less than 6 molecules in its vicinity along the edge. In view of this observation, the cut-off distance was set to δ^* to study the dependence of the line tension $k_{\bigcirc}$ and flexural rigidity k_1 on the molecular aspect ratio σ_e/σ_s. It is evident from Figure 4 that the line tension $k_{\bigcirc}$ is not as sensitive as the flexural rigidity k_1 to the molecular aspect ratio σ_e/σ_s. This difference can be quantified by considering the relative change of those quantities associated with a same increment of the molecular aspect ratio σ_e/σ_s. Further, with an increase in the aspect ratio, the line tension decreases while the flexural rigidity increases. This signals that for molecules with greater aspect ratios, inclusion of the bending contribution to the free-energy is of more significance. Considering that a rod with a larger diameter shows more resistance to bending, the observation that the flexural rigidity of the edge is greater for larger molecular aspect ratios (longer molecules lead to larger cross-sectional diameter of the edge), agrees with what would be expected intuitively.

The energy functional obtained in (30) was used to explore energy of the degenerate case of a circular pore on a spheroidal lipid bilayer, resulting in the expression (47). The pore size needs to be greater than the mean distance of molecules $\sigma_{\bigcirc}$. For such sizes, the contribution of the flexural part to the energy given by (47) is negligible, and effectively, the energy increases linearly with the pore size. Inspired by earlier investigations on rupturing of soap films [39], Litster [40] developed a continuum model for the free-energy φ needed for opening-up of a pore in a lipid membrane in the form

$$\frac{\phi}{2\pi} = \Gamma r - \frac{1}{2}\gamma_s r^2, \quad (48)$$

with Γ the line energy of the edge and γ_s the interfacial surface tension. It can be inferred from (48) that transient pores with sizes less than a critical radius $r^* = \Gamma/\gamma_s$ tend to reseal, while those having the size exceeding this critical radius, might grow indefinitely, leading to rupture of the membrane [41]. In other words, the energy to form a pore of radius r is determined by a balance between two competitive contributions: the energy required to create the edge of the pore, and the energy released by the pore surface [42]. Nevertheless, it is a common knowledge today (see for example the review by Jähnig [43]) that lipid membranes possess zero surface tension, by which the second term on the right hand of (48) vanishes. This transpires the agreement of the current result based on molecular interactions, with that obtained previously on continuum grounds. The increasing cost of generating a larger pore confirms the stability of a lipid membrane with respect to the fluctuations that might bring about transient pores. Furthermore, the growth of stable pores in homogenous lipid bilayers is only possible in the presence of external stimuli such as an electric field.

The class of the interaction potentials (23) selected in the present study and the integration (26), only account for the lipid bilayers in which the physiochemical properties of the constituent molecules are identical. An important corollary of our model would follow from a generalization of the arguments of the interaction potential (23) and the integration (26), to allow for the interactions between phospholipid molecules of different physiochemical properties. Such a generalization permits modeling perforated mixed lipid bilayers, such as those reported by Oglęcka *et al.* [44] and Jiang & Kindt [36]. Further, our model accounts for the elastic free-energy of the edge of open lipid bilayers in which the lipid molecules are tilted only at the edge, forming a semicylindrical rim along it. Another generalization of the present work would include tilt fields of smaller gradient, such as those considered by Hamm and Kozlov [45], Rangamani and Steigmann [46], and Rangamani *et al.* [47]. In such an approach, the gradual tilt at the vicinity of the edge changes the thickness of the lipid bilayer and, thus, leads to the deviation of the conformation of the edge from a semicylindrical shape. These potential generalizations remain to be investigated in future.

Acknowledgement

Financial support from National Institutes of Health (NIDCD) grant DC 005788 is gratefully acknowledged. The authors thank Mohsen Maleki for Figures 1–3.

Appendix A. Detailed derivation of (18)

Let ψ denote the angle between the unit normal **N** to the curve $\mathscr{C}$ and the unit normal $\boldsymbol{n}$ to the surface $\mathscr{S}$. The Darboux frame $\{\boldsymbol{t}, \boldsymbol{n}, \boldsymbol{p}\}$ at any point on $\mathscr{C}$, is obtained by rotating the Frenet frame $\{\boldsymbol{t}, \mathbf{N}, \mathbf{B}\}$ about the unit tangent **t** by angle. Hence,

$$\begin{bmatrix} \boldsymbol{t} \\ \boldsymbol{n} \\ \boldsymbol{p} \end{bmatrix} = \begin{bmatrix} 1 & 0 & 0 \\ 0 & cos\,\psi & sin\,\psi \\ 0 & -sin\,\psi & cos\,\psi \end{bmatrix} \begin{bmatrix} \mathbf{t} \\ \mathbf{N} \\ \mathbf{B} \end{bmatrix}. \quad \text{(A.1)}$$

Let the array $\mathbf{X} = [\boldsymbol{t}\,\boldsymbol{n}\,\boldsymbol{p}]^{\mathrm{T}}$ denote the Darboux frame, and $\mathbf{Y} = [\mathbf{t}\,\mathbf{N}\,\mathbf{B}]^{\mathrm{T}}$ denote the Frenet frame at a given point on $\mathscr{C}$, where T denotes the transpose. Also let

$$\mathbf{Q} := \begin{bmatrix} 1 & 0 & 0 \\ 0 & cos\,\psi & sin\,\psi \\ 0 & -sin\,\psi & cos\,\psi \end{bmatrix} \quad \text{(A.2)}$$

denote the transformation between the two frames. Thus,

$$\mathbf{X}=\mathbf{Q}\mathbf{Y}, \quad \text{or} \quad \boldsymbol{Y}=\mathbf{Q}^{\mathrm{T}}\mathbf{X}. \quad \text{(A.3)}$$

The derivative of the Frenet frame {**t**, **N**, **B**} of $\mathscr{C}$ with respect to the arclength *s*, follows from the Frenet-Serret formulas [48]

$$\begin{bmatrix} \dot{\mathbf{t}} \\ \dot{\mathbf{N}} \\ \dot{\mathbf{B}} \end{bmatrix} = \begin{bmatrix} 0 & \kappa & 0 \\ -\kappa & 0 & \tau \\ 0 & -\tau & 0 \end{bmatrix} \begin{bmatrix} \mathbf{t} \\ \mathbf{N} \\ \mathbf{B} \end{bmatrix}. \quad \text{(A.4)}$$

Thus,

$$\dot{\boldsymbol{Y}} = \mathbf{A}\mathbf{Y}=\mathbf{A}\mathbf{Q}^{\mathrm{T}}\mathbf{X}, \quad \text{(A.5)}$$

where

$$\mathbf{A}= \begin{bmatrix} 0 & \kappa & 0 \\ -\kappa & 0 & \tau \\ 0 & -\tau & 0 \end{bmatrix}. \quad \text{(A.6)}$$

Taking arclength derivative from both sides of $(A.3)_1$ yields

$$\dot{\mathbf{X}} = \dot{\mathbf{Q}}\,\boldsymbol{Y}+\mathbf{Q}\,\dot{\boldsymbol{Y}}, \quad \text{(A.7)}$$

where

$$\dot{\mathbf{Q}} = \begin{bmatrix} 0 & 0 & 0 \\ 0 & -\dot{\psi}\ sin\,\psi & \dot{\psi}\ cos\,\psi \\ 0 & -\dot{\psi}\ cos\,\psi & -\dot{\psi}\ sin\,\psi \end{bmatrix}. \quad \text{(A.8)}$$

In view of $(A.3)_2$ and the right-hand side of (A.5), (A.7) takes the form

$$\dot{\mathbf{X}} = \left(\dot{\mathbf{Q}}\,\mathbf{Q}^{T}+\mathbf{Q}\mathbf{A}\mathbf{Q}^{\mathrm{T}}\right)\mathbf{X}, \quad \text{(A.9)}$$

or, equivalently,

$$\begin{bmatrix} \dot{\boldsymbol{t}} \\ \dot{\boldsymbol{n}} \\ \dot{\boldsymbol{p}} \end{bmatrix} = \begin{bmatrix} 0 & \kappa\,cos\,\psi & -\kappa\,sin\,\psi \\ -\kappa\,cos\,\psi & 0 & \tau+\dot{\psi} \\ \kappa\,sin\,\psi & -\tau-\dot{\psi} & 0 \end{bmatrix} \begin{bmatrix} \boldsymbol{t} \\ \boldsymbol{n} \\ \boldsymbol{p} \end{bmatrix}. \quad \text{(A.10)}$$

In view of $\kappa_n=\kappa\,cos\,\psi$, $\kappa_g=\kappa\,sin\,\psi$, and $\tau_g=\tau+\dot{\psi}$, (A.10) simplifies to (18).

Appendix B. Derivation of the free-energy density (29)

In this Appendix, the expansion of (28) to (29) is presented. As mentioned earlier, only the molecules separated by a distance less than δ may interact. Hence, the domain of the integral with respect to t in (27) is replaced by $[-\delta,\delta]$. Upon replacing $\omega(s,\theta)$ in (28), and substituting Ω by its equivalent from (23), and applying the change of variable $t - t_\circ = s\varrho$, (28) takes the form

$$\phi=\varrho\int_{-\ell}^{\ell}\int_{\frac{-\pi}{2}}^{\frac{\pi}{2}}\tilde{\Omega}\left(\varrho^{-2}\boldsymbol{r}\cdot\boldsymbol{r},\boldsymbol{r}\cdot\boldsymbol{d}\left(t_\circ,\theta\right),\boldsymbol{r}\cdot\boldsymbol{d}\left(t_\circ+s\varrho,\eta\right),\boldsymbol{d}\left(t_\circ,\theta\right)\cdot\boldsymbol{d}\left(t_\circ+s\varrho,\eta\right)\right)\Pi\left(t_\circ\right)\Pi\left(t_\circ+s\varrho\right)\quad \mathrm{d}\eta\quad \mathrm{d}\theta\quad \mathrm{d}s. \tag{B.1}$$

It is necessary to expand the right-hand side of (B.1) in powers of ϱ neglecting terms of $o(\varrho^2)$. Introducing the abbreviations

$$\left.\begin{array}{lll}\boldsymbol{n}:=\boldsymbol{n}\left(0\right), & \boldsymbol{t}:=\boldsymbol{t}\left(0\right), & \boldsymbol{p}:=\boldsymbol{p}\left(t_\circ\right),\\ \Pi:=\Pi\left(0\right), & \dot{\Pi}:=\dot{\Pi}\left(0\right), & \ddot{\Pi}:=\ddot{\Pi}\left(0\right),\end{array}\right\} \tag{B.2}$$

and applying the identities given in (18), the following expansions up to ϱ^2 are obtained:

$$\begin{array}{ll}\boldsymbol{x}\left(s\varrho\right)= & \boldsymbol{x}\left(0\right)+\varrho s\quad \boldsymbol{t}+\frac{1}{2}s^2\varrho^2\kappa_n\quad \boldsymbol{n}-\frac{1}{2}s^2\varrho^2\kappa_g\quad \boldsymbol{p}+o\left(\varrho^4\right),\\ \boldsymbol{n}\left(s\varrho\right)= & \left(\frac{s^2\varrho^2}{2}\left(\dot{\kappa}_n-\kappa_g\tau_g\right)-s\varrho\kappa_n\right)\boldsymbol{t}+\left(1-\frac{s^2\varrho^2}{2}\left(\kappa_n^2+\tau_g^2\right)\right)\boldsymbol{n}+\left(\frac{s^2\varrho^2}{2}\left(\kappa_n\kappa_g+\dot{\tau}_g\right)+s\varrho\tau_g\right)\boldsymbol{p}+o\left(\varrho^2\right),\\ \boldsymbol{p}\left(s\varrho\right)= & \left(\frac{s^2\varrho^2}{2}\left(\kappa_n\kappa_g-\dot{\tau}_g\right)-s\varrho\tau_g\right)\boldsymbol{n}+\left(\varrho s\kappa_g+\frac{s^2\varrho^2}{2}\left(\dot{\kappa}_g+\tau_g\kappa_n\right)\right)\boldsymbol{t}+\left(1-\frac{s^2\varrho^2}{2}\left(\tau_g^2+\kappa_g^2\right)\right)\boldsymbol{p}+o\left(\varrho^2\right).\end{array} \tag{B.3}$$

Therefore, the arguments of the interaction potential $\tilde{\Omega}$ in the right-hand side of (B.1) become

$$\begin{array}{l}\varrho^{-2}\left|\boldsymbol{x}\left(t_\circ\right)-\boldsymbol{x}\left(t_\varrho\right)\right|^2=s^2+A_1\varrho^2s^4+o\left(\varrho^2\right),\\ \left(\boldsymbol{x}\left(t_\circ\right)-\boldsymbol{x}\left(t_\varrho\right)\right)\cdot\boldsymbol{d}\left(t_\circ,\theta\right)=A_2\varrho^2s^2+o\left(\varrho^2\right),\\ \left(\boldsymbol{x}\left(t_\circ\right)-\boldsymbol{x}\left(t_\varrho\right)\right)\cdot\boldsymbol{d}\left(t_\varrho,\eta\right)=A_3\varrho^2s^2+o\left(\varrho^2\right),\\ \boldsymbol{d}\left(t_\circ,\theta\right)\cdot\boldsymbol{d}\left(t_\varrho,\eta\right)=A_4+A_5\varrho s+A_6\varrho^2s^2+o\left(\varrho^2\right),\end{array} \tag{B.4}$$

where $t_\varrho = t_\circ + s\varrho$, and

$$\begin{array}{l}A_1=-\frac{\kappa^2}{12},\quad A_2=\frac{\kappa_g\,cos\,\theta-\kappa_n\,sin\,\theta}{2},\quad A_3=\frac{\kappa_n\,sin\,\eta-\kappa_g\,cos\,\eta}{2},\\ A_4=cos\left(\theta-\eta\right)\quad A_5=-\tau_g\,sin\left(\theta-\eta\right),\\ A_6=\frac{\kappa_n\kappa_g}{2}sin\left(\theta+\eta\right)-\frac{\dot{\tau}_g}{2}sin\left(\theta-\eta\right)-\frac{\tau_g^2}{2}cos\left(\theta-\eta\right)-\frac{\kappa_g^2}{2}cos\,\theta\quad cos\,\eta-\frac{\kappa_n^2}{2}sin\,\theta\quad sin\,\eta.\end{array} \tag{B.5}$$

Expanding $\tilde{\Omega}$ up to ϱ^2 and using

$$\Pi\left(s\varrho\right)=\Pi+s\varrho\,\dot{\Pi}+\frac{s^2\varrho^2}{2}\ddot{\Pi}+o\left(\varrho^2\right), \tag{B.6}$$

results in the following energy-density for the edge

$$\begin{aligned}\phi &= \int_{-\ell}^{\ell}\int_{\frac{-\pi}{2}}^{\frac{\pi}{2}}\int_{\frac{-\pi}{2}}^{\frac{\pi}{2}}\left\{\varrho\,\bar{\Omega}\,(s,\theta,\eta)\,\Pi^2 \quad \mathrm{d}\eta \quad \mathrm{d}\theta \quad \mathrm{d}s+\tfrac{1}{2}\varrho^3\,\bar{\Omega}\,(s,\theta,\eta)\,s^2\Pi\ddot{\Pi}\right\}\mathrm{d}\eta \quad \mathrm{d}\theta \quad \mathrm{d}s\\ &+\kappa_g^2\left\{\varrho^3\int_{-\ell}^{\ell}\int_{\frac{-\pi}{2}}^{\frac{\pi}{2}}\int_{\frac{-\pi}{2}}^{\frac{\pi}{2}}\frac{-s^2\Pi^2}{12}\left(\bar{\Omega}_1\,(s,\theta,\eta)\,s^2+6\,\bar{\Omega}_4\,(s,\theta,\eta)\;cos\,\theta \quad cos\,\eta\right) \quad \mathrm{d}\eta \quad \mathrm{d}\theta \quad \mathrm{d}s\right\}\\ &+\kappa_n^2\left\{\varrho^3\int_{-\ell}^{\ell}\int_{\frac{-\pi}{2}}^{\frac{\pi}{2}}\int_{\frac{-\pi}{2}}^{\frac{\pi}{2}}\frac{-s^2\Pi^2}{12}\left(\bar{\Omega}_1\,(s,\theta,\eta)\,s^2+6\,\bar{\Omega}_4\,(s,\theta,\eta)\;sin\,\theta \quad sin\,\eta\right) \quad \mathrm{d}\eta \quad \mathrm{d}\theta \quad \mathrm{d}s\right\}\\ &+\kappa_g\left\{\varrho^3\int_{-\ell}^{\ell}\int_{\frac{-\pi}{2}}^{\frac{\pi}{2}}\int_{\frac{-\pi}{2}}^{\frac{\pi}{2}}\frac{s^2\Pi^2}{2}\left(\bar{\Omega}_2\,(s,\theta,\eta)\;cos\,\theta-\bar{\Omega}_3\,(s,\theta,\eta)\;cos\,\eta\right) \quad \mathrm{d}\eta \quad \mathrm{d}\theta \quad \mathrm{d}s\right\}\\ &+\kappa_n\left\{\varrho^3\int_{-\ell}^{\ell}\int_{\frac{-\pi}{2}}^{\frac{\pi}{2}}\int_{\frac{-\pi}{2}}^{\frac{\pi}{2}}\frac{s^2\Pi^2}{2}\left(\bar{\Omega}_3\,(s,\theta,\eta)\;sin\,\eta-\bar{\Omega}_2\,(s,\theta,\eta)\;sin\,\theta\right) \quad \mathrm{d}\eta \quad \mathrm{d}\theta \quad \mathrm{d}s\right\}\\ &+\tau_g^2\left\{\varrho^3\int_{-\ell}^{\ell}\int_{\frac{-\pi}{2}}^{\frac{\pi}{2}}\int_{\frac{-\pi}{2}}^{\frac{\pi}{2}}\frac{s^2\Pi^2}{2}\left(\bar{\Omega}_{44}\,(s,\theta,\eta)\;sin^2\,(\theta-\eta)-\bar{\Omega}_4\,(s,\theta,\eta)\;cos\,(\theta-\eta)\right) \quad \mathrm{d}\eta \quad \mathrm{d}\theta \quad \mathrm{d}s\right\}\\ &+\kappa_n\kappa_g\left\{\varrho^3\int_{-\ell}^{\ell}\int_{\frac{-\pi}{2}}^{\frac{\pi}{2}}\int_{\frac{-\pi}{2}}^{\frac{\pi}{2}}\frac{s^2\Pi^2}{2}\bar{\Omega}_4\,(s,\theta,\eta) \quad sin\,(\theta+\eta) \quad \mathrm{d}\eta \quad \mathrm{d}\eta \quad \mathrm{d}s\right\},\end{aligned} \tag{B.7}$$

where

$$\left.\begin{aligned}\bar{\Omega}\,(s,\theta,\eta) &:= \tilde{\Omega}\,(s^2,0,0,cos\,(\theta-\eta))\,,\\ \bar{\Omega}_i\,(s,\theta,\eta) &:= \tilde{\Omega}_{,i}\,(s^2,0,0,cos\,(\theta-\eta))\,,\\ \bar{\Omega}_{ii}\,(s,\theta,\eta) &:= \tilde{\Omega}_{,ii}\,(s^2,0,0,cos\,(\theta-\eta))\,,\end{aligned}\right\} \quad i\in\{1,2,3,4\}\,. \tag{B.8}$$

Note that $\bar{\Omega}$, $\bar{\Omega}_i$ and $\bar{\Omega}_{ii}$ vanish when $s>\ell$. Thus, the final expression for the free-energy density of the edge becomes

$$\phi=k_\circ+k_1\kappa_g^2+k_2\kappa_n^2+k_3\kappa_g+k_4\kappa_n+k_5\kappa_n\kappa_g+k_6\tau_g^2, \tag{B.9}$$

or, equivalently,

$$\phi=k_\circ+k_1(\kappa_g-\kappa_{g\circ})^2+k_2(\kappa_n-\kappa_{n\circ})^2+k_5\kappa_n\kappa_g+k_6\tau_g^2, \tag{B.10}$$

where the parameters $k_\bigcirc$–k_6 are given by the integral representations in (B.7).

Appendix C. Integral representations I○, I and J in (40)

$$\begin{aligned}I_\circ &= \int_{\frac{-\pi}{2}}^{\frac{\pi}{2}}\int_{\frac{-\pi}{2}}^{\frac{\pi}{2}}\sqrt{1-\chi^2cos^2\,(\theta-\eta)} \quad \mathrm{d}\eta \quad \mathrm{d}\theta,\\ I &= \int_{\frac{-\pi}{2}}^{\frac{\pi}{2}}\int_{\frac{-\pi}{2}}^{\frac{\pi}{2}}\frac{1}{\sqrt{1-\chi^2cos^2(\theta-\eta)}}\mathrm{d}\eta \quad \mathrm{d}\theta,\\ J &= \int_{\frac{-\pi}{2}}^{\frac{\pi}{2}}\int_{\frac{-\pi}{2}}^{\frac{\pi}{2}}\frac{cos(2\theta-2\eta)}{\sqrt{1-\chi^2cos^2(\theta-\eta)}}\mathrm{d}\eta \quad \mathrm{d}\theta.\end{aligned} \tag{C.1}$$

References

1. Israelachvili, JN. Intermolecular and surface forces. revised third edition. Academic press; 2011.
2. Israelachvili JN, Mitchell DJ, Ninham BW. Theory of self-assembly of lipid bilayers and vesicles. Biochimica et Biophysica Acta (BBA)-Biomembranes. 1977; 470(2):185–201. [PubMed: 911827]
3. Israelachvili JN, Mitchell DJ, Ninham BW. Theory of self-assembly of hydrocarbon amphiphiles into micelles and bilayers. Journal of the Chemical Society, Faraday Transactions 2: Molecular and Chemical Physics. 1976; 72:1525–1568.

4. Lodish, HF.; Berk, A.; Zipursky, SL.; Matsudaira, P.; Baltimore, D.; Darnell, J., et al. Molecular cell biology. Vol. 4. WH Freeman; New York: 2000.
5. Saitoh A, Takiguchi K, Tanaka Y, Hotani H. Opening-up of liposomal membranes by talin. Proceedings of the National Academy of Sciences. 1998; 95(3):1026–1031.
6. Luckey, M. Membrane structural biology: with biochemical and biophysical foundations. Cambridge University Press; 2014.
7. Seifert U. Configurations of fluid membranes and vesicles. Advances in Physics. 1997; 46(1):13–137.
8. Lasic DD. The mechanism of vesicle formation. Biochemical Journal. 1988; 256(1):1. [PubMed: 3066342]
9. Tsong TY. Electroporation of cell membranes. Biophysical Journal. 1991; 60(2):297–306. [PubMed: 1912274]
10. Marmottant P, Hilgenfeldt S. Controlled vesicle deformation and lysis by single oscillating bubbles. Nature. 2003; 423(6936):153–156. [PubMed: 12736680]
11. Fromherz P, Röcker C, Rüppel D. From discoid micelles to spherical vesicles. the concept of edge activity. Faraday Discussions of the Chemical Society. 1986; 81:39–48.
12. Tu Z, Ou-Yang Z. A geometric theory on the elasticity of biomembranes. Journal of Physics A: Mathematical and General. 2004; 37(47):11407.
13. Tu Z, Ou-Yang Z. Elastic theory of low-dimensional continua and its applications in bio-and nano-structures. Journal of Computational and Theoretical Nanoscience. 2008; 5(4):422–448.
14. Boal DH, Rao M. Scaling behavior of fluid membranes in three dimensions. Physical Review A. 1992; 45(10):R6947. [PubMed: 9906842]
15. Capovilla R, Guven J, Santiago J. Lipid membranes with an edge. Physical Review E. 2002; 66(2): 021607.
16. Tu Z. Compatibility between shape equation and boundary conditions of lipid membranes with free edges. The Journal of Chemical Physics. 2010; 132(8):084111. [PubMed: 20192294]
17. Tu Z. Geometry of membranes. arXiv preprint arXiv. :1106, 2370.
18. Tu Z, Ou-Yang Z. Lipid membranes with free edges. Physical Review E. 2003; 68(6):061915.
19. May S. A molecular model for the line tension of lipid membranes. The European Physical Journal E. 2000; 3(1):37–44.
20. Keller JB, Merchant GJ. Flexural rigidity of a liquid surface. Journal of Statistical Physics. 1991; 63(5-6):1039–1051.
21. Seguin B, Fried E. Microphysical derivation of the canham–helfrich free-energy density. Journal of Mathematical Biology. 2014; 68(3):647–665. [PubMed: 23389779]
22. Asgari M. Elastic free-energy of wormlike micellar chains: theory and suggested experiments. arXiv preprint arXiv. :1502, 02338.
23. Jiang FY, Bouret Y, Kindt JT. Molecular dynamics simulations of the lipid bilayer edge. Biophysical Journal. 2004; 87(1):182–192. [PubMed: 15240456]
24. Wohlert J, Den Otter W, Edholm O, Briels W. Free energy of a trans-membrane pore calculated from atomistic molecular dynamics simulations. The Journal of Chemical Physics. 2006; 124(15): 154905. [PubMed: 16674263]
25. de Joannis J, Jiang FY, Kindt JT. Coarse-grained model simulations of mixed-lipid systems: composition and line tension of a stabilized bilayer edge. Langmuir. 2006; 22(3):998–1005. [PubMed: 16430259]
26. Karatekin E, Sandre O, Guitouni H, Borghi N, Puech P-H, Brochard-Wyart F. Cascades of transient pores in giant vesicles: line tension and transport. Biophysical Journal. 2003; 84(3):1734–1749. [PubMed: 12609875]
27. Berne BJ, Pechukas P. Gaussian model potentials for molecular interactions. The Journal of Chemical Physics. 1972; 56(8):4213–4216.
28. Gay J, Berne B. Modification of the overlap potential to mimic a linear site–site potential. The Journal of Chemical Physics. 1981; 74(6):3316–3319.
29. Guggenheimer H. Differential geometry. 1977; 1963
30. Synge, JL. Tensor calculus. Vol. 5. Courier Corporation; 1969.

31. Guven J, Huber G, Valencia DM. Terasaki spiral ramps in the rough endoplasmic reticulum. Physical Review Letters. 2014; 113(18):188101. [PubMed: 25396396]
32. Zhelev DV, Needham D. Tension-stabilized pores in giant vesicles: determination of pore size and pore line tension. Biochimica et Biophysica Acta (BBA)-Biomembranes. 1993; 1147(1):89–104. [PubMed: 8466935]
33. Truesdell, C.; Noll, W. The non-linear field theories of mechanics. Springer; 2004.
34. Whitehead L, Edge CM, Essex JW. Molecular dynamics simulation of the hydrocarbon region of a biomembrane using a reduced representation model. Journal of Computational Chemistry. 2001; 22(14):1622–1633.
35. Mashaghi A, Partovi-Azar P, Jadidi T, Nafari N, Maass P, Tabar MRR, Bonn M, Bakker HJ. Hydration strongly affects the molecular and electronic structure of membrane phospholipids. The Journal of Chemical Physics. 2012; 136(11):114709. [PubMed: 22443792]
36. Jiang Y, Kindt JT. Simulations of edge behavior in a mixed-lipid bilayer: fluctuation analysis. The Journal of Chemical Physics. 2007; 126(4):045105. [PubMed: 17286515]
37. Pera H, Kleijn J, Leermakers F. On the edge energy of lipid membranes and the thermodynamic stability of pores. The Journal of Chemical Physics. 2015; 142(3):034101. [PubMed: 25612683]
38. Biria A, Maleki M, Fried E. Continuum theory for the edge of an open lipid bilayer. Advances in Applied Mechanics. 2013; 21:1–78.
39. Deryagin B, Gutop YV. Theory of the breakdown (rupture) of free films. Kolloidn. Zh. 1962; 24:370–374.
40. Litster J. Stability of lipid bilayers and red blood cell membranes. Physics Letters A. 1975; 53(3): 193–194.
41. Deserno M. Fluid lipid membranes: From differential geometry to curvature stresses. Chemistry and Physics of Lipids.
42. Genco I, Gliozzi A, Relini A, Robello M, Scalas E. Electroporation in symmetric and asymmetric membranes. Biochimica et Biophysica Acta (BBA)-Biomembranes. 1993; 1149(1):10–18. [PubMed: 8318522]
43. Jähnig F. What is the surface tension of a lipid bilayer membrane? Biophysical Journal. 1996; 71(3):1348. [PubMed: 8874009]
44. Oglęcka K, Rangamani P, Liedberg B, Kraut RS, Parikh AN. Oscillatory phase separation in giant lipid vesicles induced by trans-membrane osmotic differentials. eLife. 2014; 3:e03695. [PubMed: 25318069]
45. Hamm M, Kozlov M. Elastic energy of tilt and bending of fluid membranes. The European Physical Journal E. 2000; 3(4):323–335.
46. Rangamani P, Steigmann D. Variable tilt on lipid membranes, Proceedings of the Royal Society A: Mathematical. Physical and Engineering Science. 2014; 470(2172):20140463.
47. Rangamani P, Benjamini A, Agrawal A, Smit B, Steigmann DJ, Oster G. Small scale membrane mechanics. Biomechanics and modeling in mechanobiology. 2014; 13(4):697–711. [PubMed: 24081650]
48. Kreyszig, E. Introduction to differential geometry and Riemannian geometry. Vol. 16. University of Toronto Press; 1968.

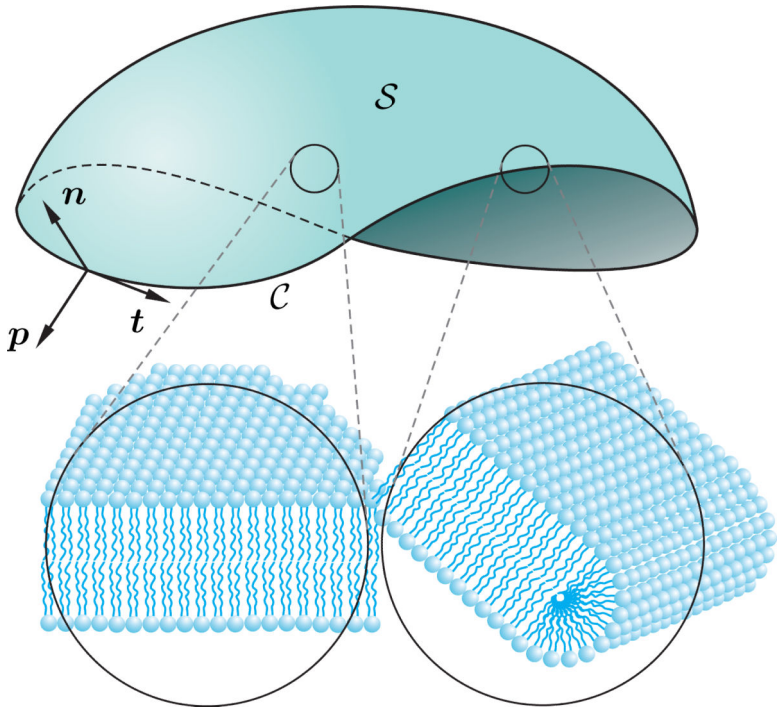

Figure 1.

Mathematical identification of an open lipid bilayer as an open surface $\mathscr{S}$ with boundary $\mathscr{C}=\partial\mathscr{S}$ on which a Darboux frame has been shown. Also the schematic arrangements of phospholipid molecules in an interior point on $\mathscr{S}$ and at the vicinity of the edge $\mathscr{C}$ are depicted at a point.

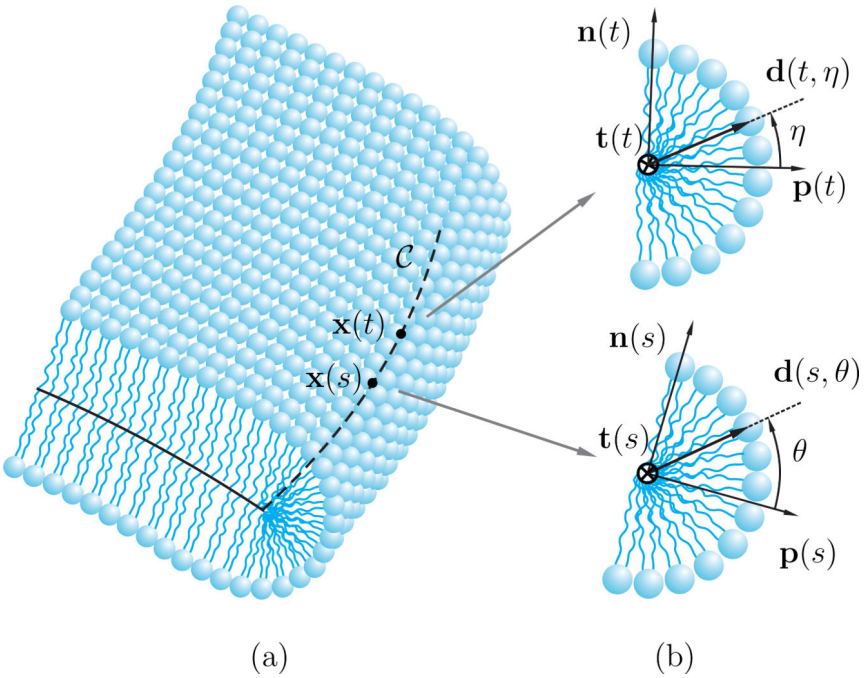

Figure 2.

(a) The schematic of a section of the edge of an open bilayer, (b) cross-sections of the edge at positions **x**(*s*) and **x**(*t*) with Darboux frame {**t**, **n**, **p**} at those positions.

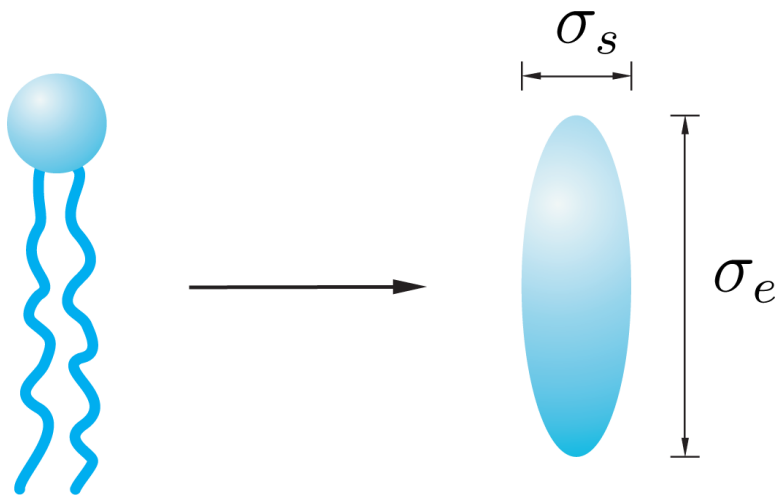

Figure 3.
(a) The schematic of a phospholipid molecule modelled as an ellipsoidal particle.

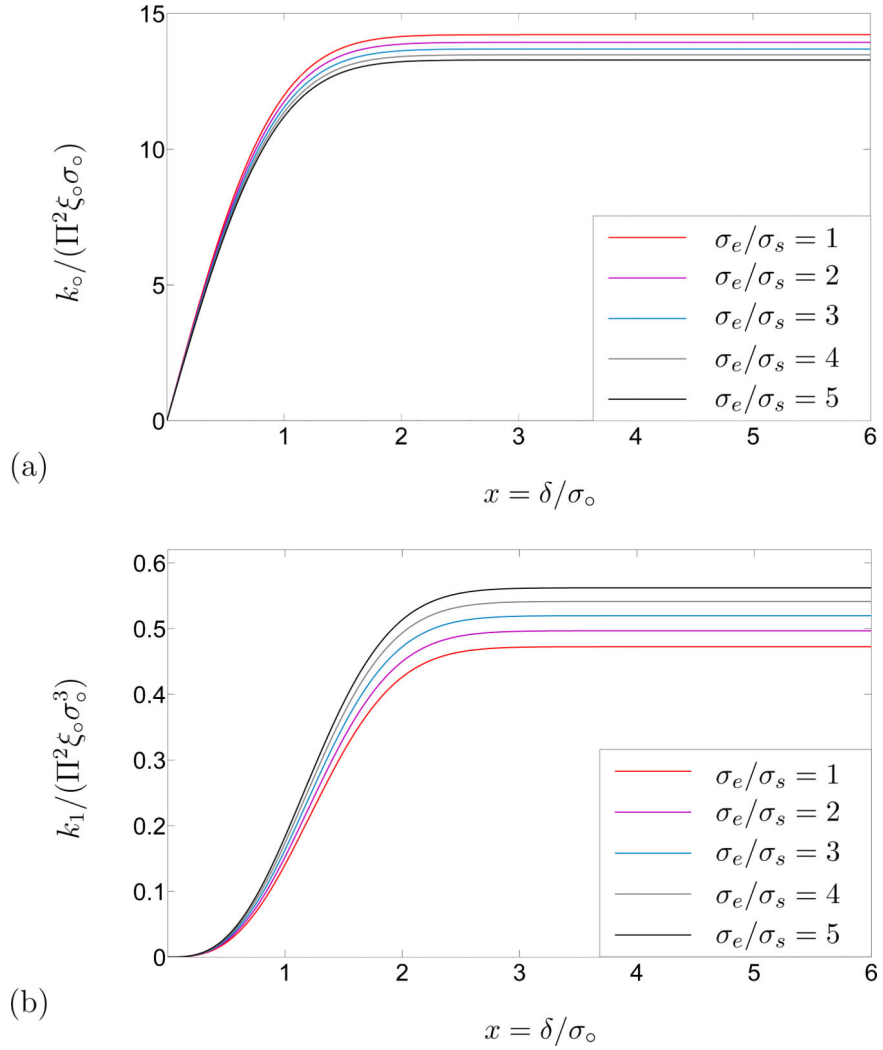

Figure 4.

(a). Schematic of the constant line energy $k_\bigcirc/\Pi^2\xi_\bigcirc\sigma_\bigcirc$ in terms of the dimensionless cut-off distance $\delta/\sigma_\bigcirc$. (b) Schematic of the flexural rigidity $k_1/\Pi^2\xi_\circ\sigma_\circ^3$ in terms of the dimensionless cut-off distance $\delta/\sigma_\bigcirc$. As is evident from the plots, the change in $k_\bigcirc/\Pi^2\xi_\bigcirc\sigma_\bigcirc$ and $k_1/\Pi^2\xi_\circ\sigma_\circ^3$ is negligible after $\delta = 3\sigma_\bigcirc$. Consequently, the effective cut-off distance after which the potential decays rapidly, can be reasonably approximated by $\delta = 3\sigma_\bigcirc$.

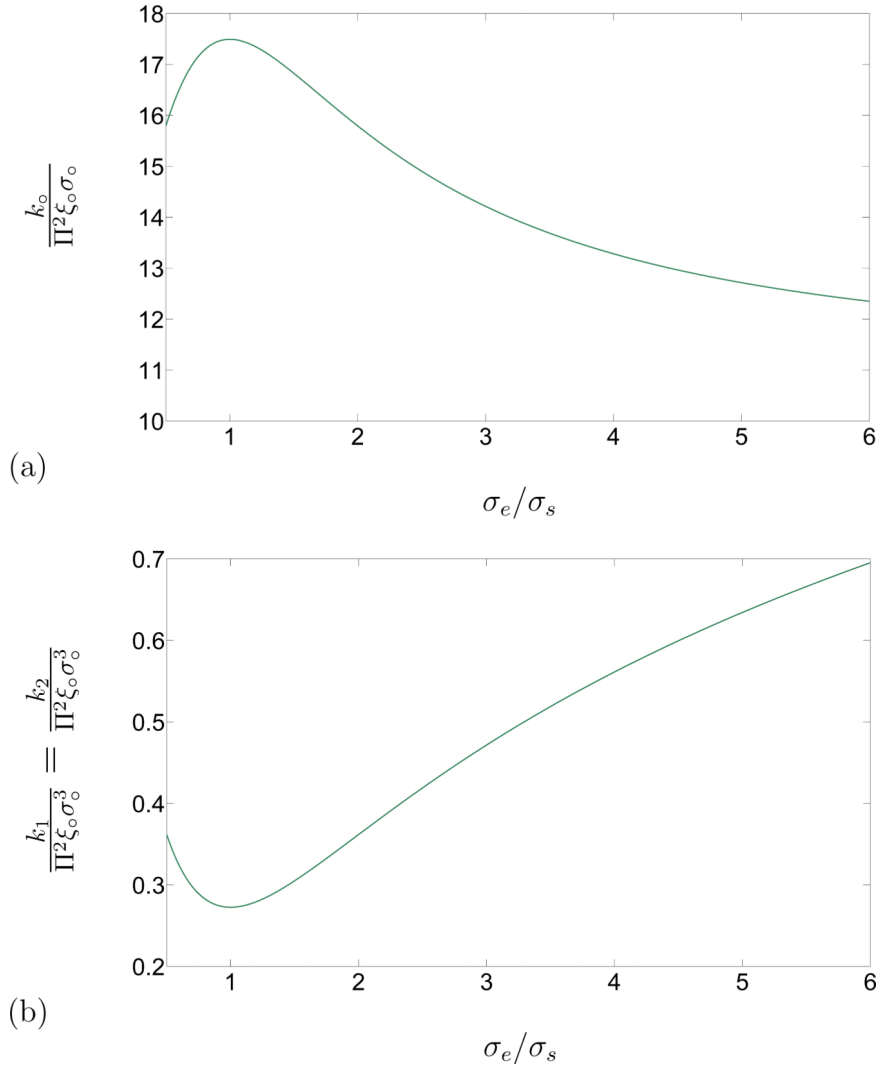

Figure 5.

(a). Schematic of the constant line energy $k_{\bigcirc}/\Pi^2\xi_{\bigcirc}\sigma_{\bigcirc}$ in terms of the aspect ratio σ_e/σ_s for a cut-off distance $\delta/\sigma_{\bigcirc} = 3$. (b) Schematic of the flexural rigidity $k_1/\Pi^2\xi_{\bigcirc}\sigma_{\bigcirc}$ in terms of the aspect ratio σ_e/σ_s for the cut-off distance $\delta = 3\sigma_{\bigcirc}$.

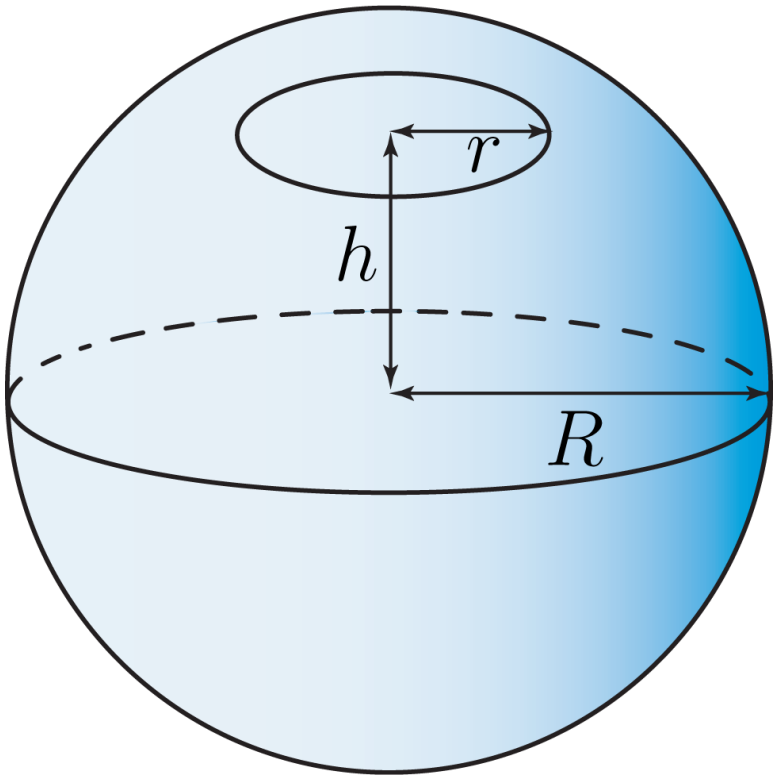

Figure 6.
Schematic of a pore on a spheroidal lipid bilayer

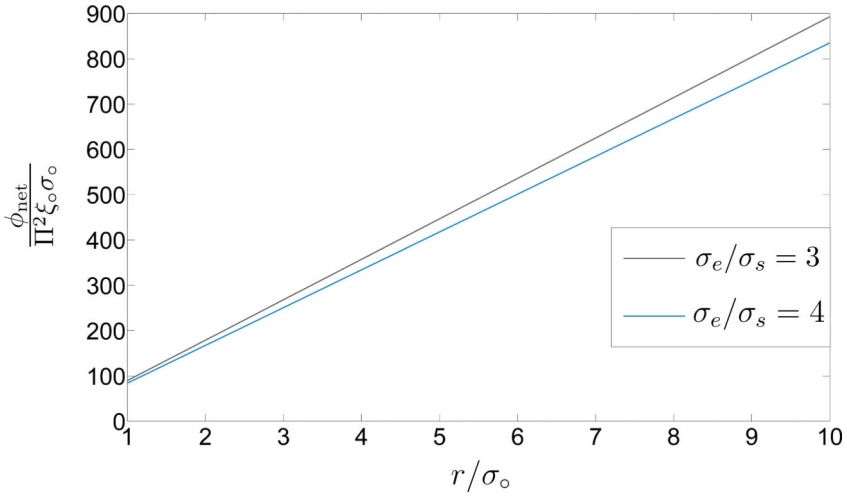

Figure 7.

Schematic of the net free-energy $\varphi_{net}/\Pi^2\xi_{\bigcirc}\sigma_{\bigcirc}$ versus the scaled pore-size $r/\sigma_{\bigcirc}$ for two values of the aspect ratio σ_e/σ_s and for the scaled cutoff distance $\delta = 3\sigma_{\bigcirc}$.